Coulomb excitation at intermediate energies

H. Esbensen
Physics Division, Argonne National Laboratory, Argonne, Illinois 60439, USA
(Received 6 July 2008; published 28 August 2008)

Straight line trajectories are commonly used in semiclassical calculations of the first-order Coulomb excitation cross section at intermediate energies, and simple corrections are often made for the distortion of the trajectories that is caused by the Coulomb field. These approximations are tested by comparing to numerical calculations that use exact Coulomb trajectories. In this paper a model is devised for including relativistic effects in the calculations. It converges at high energies toward the relativistic straight-line trajectory approximation and approaches the nonrelativistic Coulomb trajectory calculation at low energies. The model is tested against a number of measurements and analyses that have been performed at beam energies between 30 and 70 MeV/nucleon, primarily of quadrupole excitations. Remarkably good agreement is achieved with the previous analyses, and good agreement is also achieved in the few cases, where the $B(E\lambda)$ value is known from other methods. The magnitudes of the relativistic and Coulomb distortion effects are discussed.

DOI: 10.1103/PhysRevC.78.024608 PACS number(s): 23.20.−g, 25.70.De

I. INTRODUCTION

The first-order excitation of a nucleus, induced by the Coulomb field from another nucleus, has been discussed in detail in Ref. [1]. The semiclassical perturbation theory developed there was based on a classical, nonrelativistic Coulomb orbit for the relative motion of the projectile and target nuclei. A relativistic description was later developed but it was restricted to straight-line trajectories [2]. This leaves a gap in the theoretical description at intermediate energies (say, at 20–200 MeV/nucleon), where both relativistic effects and Coulomb distortions of the trajectory can be important. This is very unfortunate because many experiments have been performed in recent years at intermediate-energy, radioactive beam facilities. These include Coulomb dissociation experiments, for example, of ^{8}B, ^{11}Be and ^{11}Li, and Coulomb excitation measurements in inverse kinematics, mostly of the lowest 2^{+} state in light and medium heavy nuclei [3].

The purpose of this paper is to devise a model that interpolates smoothly between the nonrelativistic description of the Coulomb excitation which is based on Coulomb trajectories [1] and the relativistic description which is based on straight-line trajectories [2]. To develop an exact theory that contains the two extreme descriptions as limits is in general a difficult task. It has been studied by Bertulani *et al.* [4,5], who considered the effects of retardation explicitly for a Coulomb trajectory. The method proposed here is much simpler but it is sufficiently accurate for analyzing the data that have been obtained at intermediate energies. The point is that the experimental uncertainties are often large, typically of the order of 10%, and there are also theoretical uncertainties, which can distort the analysis of data, for example, the influence of nuclear and higher-order processes.

The accuracy of the proposed model of the intermediate-energy Coulomb excitation is tested by analyzing the results obtained with the commonly used 'Coulomb corrected' straight-line trajectory method, which originally was proposed by Winther and Alder [2]. Another test is to use $B(E2)$ values that are known from other measurements (for example, of the lifetime) and compare the calculated cross sections to measurements that have been performed at intermediate energies.

There has recently been a debate in the literature [6,7] about the validity of the analyses of Coulomb excitation experiments that have been performed in the past. It turned out to be caused by a misunderstanding of the experimental conditions, as pointed out in Ref. [7]. However, independent of the controversy, it was claimed that corrections to the low-energy and high-energy theories of Coulomb excitation could be as large as 20% or 30% at intermediate energies [5,6]. In this paper it will be shown how this large uncertainty can be brought under control and reduced to only a few percent.

The semiclassical theory of the nonrelativistic Coulomb excitation is summarized in Secs. II to III. The expressions that are obtained from straight-line and Coulomb trajectories, respectively, are compared in Sec. IV. The analytic expression for the relativistic Coulomb excitation in the straight line trajectory approximation is quoted in Sec. V, and it is used to devise a model which includes the combined effect of relativity and Coulomb trajectories. The model is tested in Sec. VI against measurements and other calculations, and Sec. VII contains the conclusions.

II. NONRELATIVISTIC COULOMB EXCITATION

The semiclassical, nonrelativistic description of Coulomb excitation [1] is summarized in the following. Thus we consider a target nucleus with atomic number Z_2 which is being excited by the Coulomb field from a projectile nucleus with atomic number Z_1. It is assumed that the projectile and target do not overlap during the collision. We can therefore use the so-called far-field approximation which assumes that the intrinsic coordinate r of the target nucleus is smaller that the distance $R(t)$ between projectile and target. The first-order amplitude for the electric excitation of the target nucleus, from an initial state $|i\rangle$ to a final state $|f\rangle$, is given by the multipole

expansion [1]

$$a_{fi} = \frac{Z_1 e^2}{i\hbar} \sum_{\lambda\mu} \sqrt{\frac{4\pi}{2\lambda+1}} S_{\lambda\mu}(\omega) \langle f | M^*_{\lambda\mu} | i \rangle, \tag{1}$$

where $\hbar\omega = \Delta E_{fi}$ is the excitation energy, $M_{\lambda\mu}$ is the multipole operator $r^\lambda Y_{\lambda\mu}(\hat{r})$, and

$$S_{\lambda\mu}(\omega) = \sqrt{\frac{4\pi}{2\lambda+1}} \int_{-\infty}^{\infty} dt e^{i\omega t} \frac{Y_{\lambda\mu}(\hat{R}(t))}{R(t)^{\lambda+1}} = \int_{-\infty}^{\infty} dt\, e^{i\omega t} \frac{d^\lambda_{\mu 0}(\beta) e^{i\mu\phi}}{(R(t))^{\lambda+1}} \tag{2}$$

is the so-called orbital integral. It depends on the orbit $\vec{R}(t)$ of the projectile with respect to the target nucleus. The unit vector $\hat{R} = \vec{R}/R$ is expressed in terms of the spherical coordinates (β, ϕ) in the last expression. It is noted that this definition of the orbital integral, Eq. (2), differs by the factor $\sqrt{4\pi/(2\lambda+1)}$ from the convention used in Ref. [1].

The calculation of the orbital integrals is discussed in the following sections for two choices of the coordinate system. The first choice, system A, is the most convenient for numerical calculations that are based on a Coulomb orbit [1]. The second choice, referred to as system H, is more convenient at high energies, where a straight line trajectory becomes an accurate approximation and relativistic effects can be treated exactly [2]. The transformation between the two representations will be discussed in order to be able to compare the two extreme methods and devise a model that interpolates smoothly between them.

A. Cross sections

The Coulomb excitation cross section is calculated as the product of the first-order excitation probability P_{fi} and the elastic Rutherford cross section $(d\sigma/d\Omega)_R$,

$$\left(\frac{d\sigma}{d\Omega}\right)_{fi} = P_{fi} \left(\frac{d\sigma}{d\Omega}\right)_{\mathrm{R}}. \tag{3}$$

The Rutherford cross section can be obtained from the Rutherford scattering formula, $\tan(\theta/2) = a/b$, where b is the impact parameter and

$$a = \frac{Z_1 Z_2 e^2}{M_0 v^2}, \tag{4}$$

is half the of distance of closest approach in a head-on collision, and M_0 is the reduced mass, $M_0 = M_1 M_2/(M_1 + M_2)$. The Rutherford cross section is

$$\left(\frac{d\sigma}{d\Omega}\right)_{\mathrm{R}} = \frac{2\pi b db}{d\Omega} = \pi a^2 \frac{d}{d\Omega}\left(\frac{1}{\sin^2(\theta/2)}\right). \tag{5}$$

The average excitation probability obtained from Eq. (1) is the average over the initial magnetic substates M_i and the sum over the final m-substates M_f,

$$P_{fi} = \frac{4\pi Z_1^2 e^4}{(2\lambda+1)\hbar^2} \sum_{\mu} |S_{\lambda\mu}|^2 \frac{1}{2I_i+1} \times \sum_{M_i M_f} |\langle I_f M_f | M^*_{\lambda\mu} | I_i M_i \rangle|^2.$$

The last sum divided by $(2I_i + 1)$ is equal to $(2\lambda+1)^{-1}$ times the multipole strength (or reduced transition probability) for the excitation, i.e.,

$$P_{fi} = 4\pi \left(\frac{Z_1 e^2}{(2\lambda+1)\hbar}\right)^2 B(E\lambda) \sum_{\mu} |S_{\lambda\mu}|^2. \tag{6}$$

III. ORBITAL INTEGRALS IN COORDINATE SYSTEM A

In the coordinate system denoted by A (c.f. Ref. [1]), the z-axis is perpendicular to the scattering plane so the orbit has the form $\vec{R}(t) = (x(t), y(t), 0)$. The angle β is fixed at $\pi/2$, and the orbital integral (2) can be written as

$$S^A_{\lambda\mu} = d^\lambda_{\mu 0}\left(\frac{\pi}{2}\right) \int_{-\infty}^{\infty} dt\, e^{i\omega t} \frac{(x(t) + iy(t))^\mu}{(R(t))^{\lambda+\mu+1}}. \tag{7}$$

The factor $d^\lambda_{\mu 0}(\pi/2)$ ensures that the orbital integral is nonzero only when $\lambda + \mu$ is even.

In the coordinate system A one chooses the x-axis as the symmetry axis of the Coulomb orbit so that $x(-t) = x(t)$ and $y(-t) = -y(t)$. From this it follows that $S^A_{\lambda\mu} = (S^A_{\lambda\mu})^*$ is a real quantity. To calculate $S^A_{\lambda-\mu}$ when $\mu > 0$ one can use the expression

$$S^A_{\lambda-\mu} = d^\lambda_{\mu 0}\left(\frac{\pi}{2}\right) \int_{-\infty}^{\infty} dt\, e^{i\omega t} \frac{(x(t) - iy(t))^\mu}{(R(t))^{\lambda+\mu+1}}. \tag{8}$$

Below we discuss the calculation for a Coulomb trajectory and compare it to the result of the straight-line approximation.

A. Coulomb trajectories

To evaluate the orbital integrals numerically for a Coulomb orbit one makes use of a dimensionless time-variable w (see Ref. [1]) so that

$$R(t) = a[\epsilon \cosh(w) + 1], \quad t = \frac{a}{v}[\epsilon \sinh(w) + w], \tag{9}$$

where a is defined in Eq. (4) and ϵ is the eccentricity of the orbit, which can be expressed in terms of the impact parameter b or the scattering angle θ in the center of mass system as follows:

$$\epsilon = \sqrt{1 + (b/a)^2} = \frac{1}{\sin(\theta/2)}. \tag{10}$$

Inserting the Cartesian coordinates of the orbit (see [1]):

$$x = a[\cosh(w) + \epsilon], \quad y = a\sqrt{\epsilon^2 - 1}\sinh(w), \quad z = 0, \tag{11}$$

into Eq. (7) one obtains

$$S^A_{\lambda\mu} = \frac{1}{va^\lambda} d^\lambda_{\mu 0}\left(\frac{\pi}{2}\right) I_{\lambda\mu}, \tag{12}$$

where

$$I_{\lambda\mu} = \int_{-\infty}^{\infty} dw \exp[i\xi_a(\epsilon \sinh(w) + w)] \times \frac{[\cosh(w) + \epsilon + i\sqrt{\epsilon^2 - 1}\sinh(w)]^{\mu}}{(\epsilon \cosh(w) + 1)^{\lambda+\mu}}, \quad (13)$$

and $\xi_a = \omega a/v$. Properties and even tabulations of $I_{\lambda\mu}$ are given in Ref. [8]. It will be calculated using a simple numerical integration with respect to w over the finite interval $[-5 : 5]$, and using just a few thousand steps. The accuracy of the numerical integration can be tested in the case of a straight-line trajectory against the analytic expressions, which are discussed in Appendix A.

IV. COORDINATE SYSTEM H

At high energies it is more convenient to use the coordinates system H where the z-axis is along the beam direction and the x-axis is along the impact parameter so that the y-axis is perpendicular to the scattering plane. The coordinates of the trajectory are therefore $\vec{R}(t) = (x(t), 0, z(t))$, which implies that $Y_{\lambda\mu}(\hat{R})$ is real. Since $Y^*_{\lambda\mu} = (-1)^{\mu} Y_{\lambda-\mu}$, it follows directly from the definition (2) that the orbital integral in coordinate system H must have the property

$$S^H_{\lambda-\mu}(\omega) = (-1)^{\mu} S^H_{\lambda\mu}(\omega). \quad (14)$$

The coordinate system H is convenient at high energies because the analytic expressions for the orbital integrals that exist for straight-line trajectories are relatively simple in this representation even when the relativistic effects are included [2]. This feature will be exploited in Sec. V to devise an expression that contains the effects of relativity and the Coulomb distortion of the trajectory. To do that, we will need to transform the orbital integrals in coordinate system A to the new coordinate system H.

To go from the H to the A coordinate system consists of a rotation of $\pi/2$ around the z-axis, followed by a rotation of $-\pi/2$ around the new y-axis, and finally a rotation of $-\pi/2$ around the final z-axis. The required transformation is therefore

$$S^H_{\lambda\mu} = \sum_{\mu'} i^{\mu-\mu'} d^{\lambda}_{\mu\mu'}\left(-\frac{\pi}{2}\right) S^A_{\lambda\mu'}. \quad (15)$$

Inserting Eq. (12) into this transformation we can write that

$$S^H_{\lambda\mu} = \frac{i^{\lambda+\mu}}{va^{\lambda}} I^H_{\lambda\mu},$$

where

$$I^H_{\lambda\mu} = \sum_{\mu'} i^{-(\lambda+\mu')} d^{\lambda}_{\mu'\mu}\left(\frac{\pi}{2}\right) d^{\lambda}_{\mu'0}\left(\frac{\pi}{2}\right) I_{\lambda\mu'}. \quad (16)$$

Values of $d^{\lambda}_{\mu'\mu}(\pi/2)$ can be obtained from appendix D of Ref. [1]. The explicit expressions one obtains for dipole and quadrupole excitations are

$$I^H_{10} = \frac{I_{1-1} - I_{11}}{2}, \quad I^H_{11} = \frac{I_{1-1} + I_{11}}{2\sqrt{2}}, \quad (17)$$

$$I^H_{20} = \frac{3}{8}\left[I_{22} + I_{2-2} - \frac{2}{3} I_{20}\right], \quad I^H_{21} = \frac{1}{2}\sqrt{\frac{3}{8}}[I_{2-2} - I_{22}], \quad (18)$$

$$I^H_{22} = \frac{1}{4}\sqrt{\frac{3}{8}}[I_{22} + I_{2-2} + 2I_{20}].$$

A. Straight-line trajectories

In the straight-line trajectory approximation, the projectile moves with constant velocity v along the z-axis at an impact parameter b with respect to the target, $\vec{R}(t) = (b, 0, vt)$. The nonrelativistic orbital integrals have the analytic form [2]

$$\tilde{S}^H_{\lambda\mu} = \frac{2}{v} \frac{i^{\lambda+\mu}}{\sqrt{(\lambda+\mu)!(\lambda-\mu)!}} \left(\frac{\omega}{v}\right)^{\lambda} K_{\mu}(\xi_b), \quad (19)$$

where $\xi_b = \omega b/v$ is the adiabaticity parameter associated with the impact parameter b. The tilde on $\tilde{S}^H_{\lambda\mu}$ is a reminder of the straight-line trajectory approximation, and the superscript H refers to the coordinate system used here. It should be emphasized that the expression Eq. (19) can be derived by inserting the straight-line approximation, Eq. (A3), into the transformation, Eq. (16).

B. Coulomb trajectories

In order to test the accuracy of Eq. (19) it is useful to write the general Coulomb trajectory result, Eq. (16), in a similar form,

$$S^H_{\lambda\mu} = \frac{2}{v} \frac{i^{\lambda+\mu}}{\sqrt{(\lambda+\mu)!(\lambda-\mu)!}} \left(\frac{\omega}{v}\right)^{\lambda} K^{\rm eff}_{\lambda\mu}(b/a, \xi_a), \quad (20)$$

where

$$K^{\rm eff}_{\lambda\mu}(b/a, \xi_a) = \frac{1}{2}\left(\frac{1}{\xi_a}\right)^{\lambda} \sqrt{(\lambda+\mu)!(\lambda-\mu)!}\, I^H_{\lambda\mu}, \quad (21)$$

and $I^H_{\lambda\mu}$ are the orbital integrals defined in coordinate system H according to Eq. (16). They are given explicitly by Eqs. (17) and (18) for dipole and quadrupole excitations.

One can check that $K^{\rm eff}_{\lambda\mu}$ gives the correct modified Bessel function $K_{\mu}(\xi)$ when one inserts the straight-line trajectory results in coordinate system A, Eqs. (A4)–(A6) of Appendix A, into the definition (16) of $I^H_{\lambda\mu}$. In the limit: $\xi_a \ll 1$ and $b/a \gg 1$, i.e., at high energies and large impact parameters, one should recover the result for a straight line, i.e. $K^{\rm eff}_{\lambda\mu}(b/a, \xi_a) \to K_{\mu}(\xi_b)$. This convergence will be illustrated in the next section.

To evaluate the excitation probability (6), we need the expression

$$\sum_{\mu} \left|S^H_{\lambda\mu}\right|^2 = \frac{4}{v^2 b^{2\lambda}} F_{\lambda}(b/a, \xi_a),$$

where

$$F_{\lambda}(b/a, \xi_a) = \sum_{\mu} \frac{\xi_b^{2\lambda}}{(\lambda+\mu)!(\lambda-\mu)!} \left(K^{\rm eff}_{\lambda\mu}(b/a, \xi_a)\right)^2. \quad (22)$$

In the straight-line trajectory approximation, where $K^{\rm eff}_{\lambda\mu}(b/a, \xi_a) \to K_\mu(\xi_b)$, one obtains

$$F_1(\xi_b) = \xi_b^2(K_0^2(\xi_b) + K_1^2(\xi_b)),$$

and

$$F_2(\xi_b) = \frac{\xi_b^4}{12}\big(3K_0^2(\xi_b) + 4K_1^2(\xi_b) + K_2^2(\xi_b)\big). \qquad (23)$$

for dipole and quadrupole excitations, respectively. For $\xi_b \to 0$ these functions approach the constant values $F_1 \to 1$ and $F_2 \to 1/3$.

C. Comparison of results

Here the convergence of the Coulomb trajectory calculations toward the straight-line trajectory calculation is illustrated by comparing the functions $F_\lambda(b/a, \xi_a)$ defined in Eq. (22) to the analytic expressions (23) for dipole and quadrupole excitations. The solid curves in Fig. 1 show the results of the straight-line trajectory approximation, Eq. (23), for dipole ($\lambda = 1$) and quadrupole ($\lambda = 2$) excitations, respectively, as functions of the adiabaticity parameter $\xi_b = \omega b/v$. The results of the Coulomb trajectory calculations defined in Eq. (22) are shown by dashed curves for three values of b/a. It is seen that the Coulomb trajectory results approach the straight-line result in a smooth manner for increasing values of b/a.

The solid circles in Fig. 1 are the results one obtains by multiplying the straight-line trajectory expressions, Eq. (23), with the factor $\exp(-\pi\xi_a) = \exp(-\pi\xi_b a/b)$ for $b/a = 5$. This correction factor was suggested by Winther and Alder [2] and it is seen to reproduce the dipole results ($\lambda = 1$) for the Coulomb trajectory with $b/a = 5$ fairly well. However, it does not work so well for quadrupole excitations ($\lambda = 2$). The problem is that the Coulomb trajectory results depend on b/a for $\xi_b \to 0$, whereas the simple correction factor $\exp(-\pi\xi_a) = \exp(-\pi\xi_b a/b)$ is 1 in this limit.

The nonrelativistic cross sections one obtains for the dipole excitation of the ^{11}Be $1/2^+$ ground state to the $1/2^-$ excited state and for the quadrupole excitation of ^{42}S to the 2^+ state are illustrated in Fig. 2. The cross sections were calculated for a gold target with a minimum impact parameter of 14 fm and they are shown as functions of the beam energy. Although these cross sections are referred to as nonrelativistic, it should be emphasized that the velocity that has been used here was actually obtained from the relativistic expression, Eq. (B1), in terms of the beam energy.

The excitation energies and $B(E\lambda)$ values that have been used for ^{11}Be and ^{42}S are shown in Table I, which will be

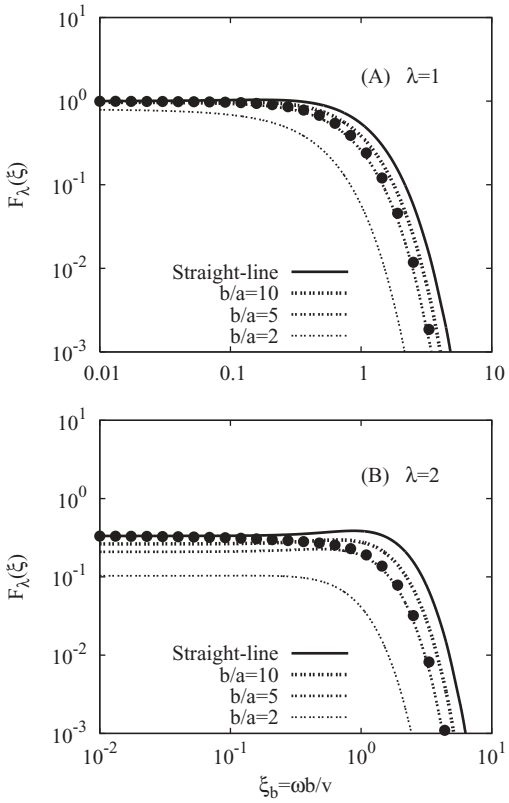

FIG. 1. The adiabaticity functions $F_\lambda(b/a, \xi)$ are illustrated for $\lambda = 1$ and 2. The top solid curves are the results for a straight line trajectory, Eq. (23). The dashed curves are obtained from Coulomb trajectories, Eq. (22), using the indicated values of b/a. The solid points were obtained by multiplying the straight line trajectory with $\exp(-\pi\xi_a) = \exp(-\pi\frac{a}{b}\xi_b)$ for $a/b = 5$.

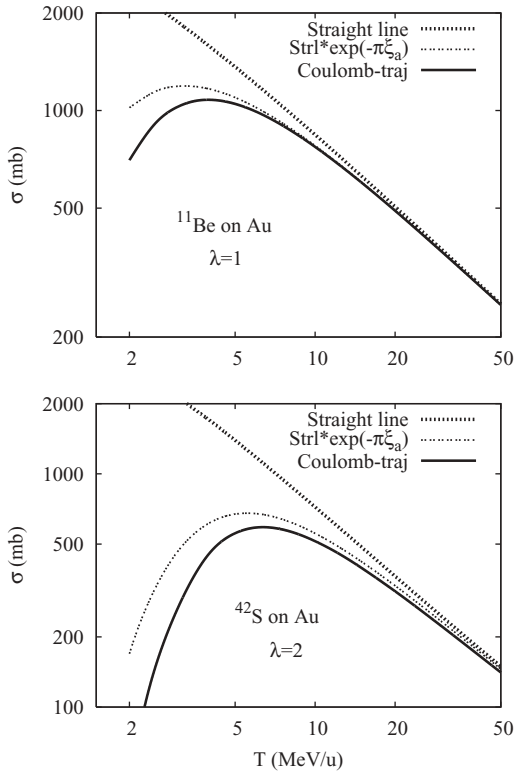

FIG. 2. Energy dependence of the nonrelativistic cross sections for the dipole excitation of ^{11}Be and the quadrupole excitation of ^{42}S discussed in the text. The target is gold, and the minimum impact parameter was set to 14 fm in both cases. The upper thick dashed curves show the straight-line trajectory approximation, whereas the thin dashed curves have been corrected with the factor $\exp(-\pi\xi_a)$. The solid curves are the results for Coulomb trajectories.

TABLE I. Cross sections for the quadrupole excitation ($\lambda = 2$) of different nuclei on a Au or Bi target, and the dipole excitation ($\lambda = 1$) of ^{11}Be (last row). The experimental conditions are from the quoted references. The T is the beam energy per nucleon at midtarget and $\phi^{\rm Lab}_{\rm max}$ ($\theta^{\rm c.m.}_{\rm max}$) is the maximum laboratory (center-of-mass) acceptance angle. The adopted $B(E2)$ values [10] for ^{24}Mg and ^{26}Mg are also shown. The the last two columns show the calculated cross sections for the relativistic Coulomb ($\sigma_{\rm Coul}$) and straight-line ($\sigma_{\rm Strl}$) trajectories.

Run no.	Nucleus	E_x (MeV)	$B(E\lambda)$ (e^2fm$^{2\lambda}$)	T (MeV/nucleon)	$\phi^{\rm Lab}_{\rm max}$ (deg)	$\sigma_{\rm exp}$ (mb)	$\sigma_{\rm Coul}$ (mb)	$\sigma_{\rm Strl}$ (mb)
0	^{24}Mg + Au [9]	1.3687	467(28)	36	$\theta^{\rm c.m.}_{\rm max} \leqslant 4.48$	78.7(48)	81.7	88.0
	adopted [10]		436(10)				76.3(18)	82.2
0	^{26}Si + Au [9]	1.7959	336(33)	41.8	$\theta^{\rm c.m.}_{\rm max} \leqslant 4.48$	55.8(55)	56.3	61.0
1	^{26}Mg + Bi [11]	1.8087	315	67	2.38	44(2)	45.9	47.8
	adopted [10]		307(9)				44.7(13)	46.6
2	^{32}Mg + Au [11]	0.885	447	71.2	2.26	91(10)	92.7	95.9
3	^{34}Mg + Bi [11]	0.659	541	67	2.38	126(22)	130.1	134.9
4	^{38}S + Au [12]	1.292	235	34.6	4.10	59(7)	60.1	64.7
5	^{40}S + Au [12]	0.891	334	35.3	4.10	94(9)	96.9	103.4
6	^{42}S + Au [12]	0.890	397	36.6	4.10	128(19)	131.1	139.9
7	^{44}Ar + Au [12]	1.144	345	30.9	4.10	81(9)	83.0	89.6
8	^{46}Ar + Au [12]	1.554	196	32.8	4.10	53(10)	53.6	58.3
9	^{46}Ar + Au [13]	1.554	212	73.2	2.90	68(8)	68.6	71.9
	^{11}Be + Au [14]	0.32	0.079	57.6	3.80	244(31)	246.1	247.2

discussed later. The top dashed curves in Fig. 2 show the straight-line trajectory calculations, and the thin dashed curves are the same results multiplied by the factor $\exp(-\pi\xi_a)$. The solid curves are based on Coulomb trajectories. They approach the straight-line trajectory approximation fairly quickly for the dipole excitation but somewhat slower for the quadrupole excitation. It is also seen that the approximation of multiplying the straight line calculation with the factor $\exp(-\pi\xi_a)$ works quite well for the dipole excitation when compared with the Coulomb trajectory calculation, whereas this approximation is poorer for quadrupole excitations. Other approximations have been applied to correct the straight line trajectory approximation for the distortion that is caused by a Coulomb trajectory and some of them will be discussed in Sec. VI D.

V. RELATIVISTIC EXPRESSION

The relativistic expressions for the orbital integrals in the straight-line trajectory approximation are [2]

$$\tilde{S}^H_{\lambda\mu}(\text{rel}) = \frac{2}{\gamma v}\frac{i^{\lambda+\mu}\bar{G}_{\lambda\mu}}{\sqrt{(\lambda+\mu)!(\lambda-\mu)!}}\left(\frac{\omega}{v}\right)^{\lambda} K_\mu\left(\xi_b = \frac{\omega b}{\gamma v}\right), \tag{24}$$

where $\bar{G}_{\lambda\mu}$ can be extracted from Ref. [2]. The notation used here is such that $\bar{G}_{\lambda\mu} = 1$ in the nonrelativistic limit, whereas Ref. [2] uses a different normalization. For electric dipole and quadrupole excitations one finds that

$$\bar{G}_{10} = \bar{G}_{20} = \bar{G}_{2\pm2} = \frac{1}{\gamma}, \quad \bar{G}_{1\pm1} = 1, \qquad \bar{G}_{2\pm1} = \frac{1}{2}\left(1 + \frac{1}{\gamma^2}\right). \tag{25}$$

It is seen that the relativistic effects on the Coulomb excitation enter into Eq. (24) through the factor $\gamma^{-1}\widetilde{G}_{\lambda\mu}$, and in the adiabatic distance $\gamma v/\omega$ of the adiabaticity parameter $\xi_b = \omega b/(\gamma v)$, which is the argument of the modified Bessel functions.

To complete the discussion of relativistic effects one should also specify the kinematics of Coulomb scattering at relativistic energies. This is done in Appendix B. One of the reasons large relativistic effects have been observed is actually due to the difference between relativistic and nonrelativistic kinematics, the main one being the determination of the velocity from the beam energy, Eq. (B1). A relativistic effect in Coulomb scattering is the γ-factor which appears in the definition (B3) of half the distance of closest approach. This effect is commonly agreed upon [2,5]. There is also a relativistic correction to the reduced mass, Eq. (B2), which is less significant at intermediate energies, and it is usually ignored [2,5]. However, for completeness, it is better to keep it in the case of really high energies. Finally, there are also relativistic effects in the transformation (B4) from the center-of-mass to laboratory scattering angles.

A. Interpolating model

To accurately calculate the Coulomb excitation at intermediate beam energies it is important to include relativistic effects and the effect of the Coulomb distortion on the relative trajectory of projectile and target. It may be difficult to derive in a general expression for the Coulomb excitation amplitude because of the acceleration in a Coulomb orbit. However, one can devise a formula which gives the correct expression in the nonrelativistic regime for a Coulomb orbit, and which reproduces the relativistic expressions for a straight-line trajectory in the high-energy regime. We shall see that the

following expression:

$$S^H_{\lambda\mu}(\text{rel}) = \frac{2}{\gamma v}\frac{i^{\lambda+\mu}\bar{G}_{\lambda\mu}}{\sqrt{(\lambda+\mu)!(\lambda-\mu)!}}\left(\frac{\omega}{v}\right)^{\lambda} \times K^{\text{eff}}_{\lambda\mu}\left(b/a, \xi_a = \frac{\omega a}{\gamma v}\right), \quad (26)$$

serves the purpose of interpolating between the two energy regimes.

It is first noted that Eq. (26) is identical to Eq. (20) if we insert $\gamma = 1$. The low-energy regime is therefore correctly described. In the high-energy regime, we can assume that $b/a \gg 1$ and $\xi_a \ll 1$, which implies that the straight-line trajectory limit will be reached,

$$K^{\text{eff}}_{\lambda\mu}(b/a, \xi_a) \to K_\mu(\xi_b), \quad \text{where} \quad \xi_b = \frac{b}{a}\xi_a,$$

according to the discussions in Secs. IV B and IV C. Since the value of ξ_a in Eq. (26) is chosen as $\xi_a = \omega a/(\gamma v)$ we obtain

$$\xi_b = \frac{b}{a} \times \frac{\omega a}{\gamma v} = \frac{\omega b}{\gamma v},$$

which is the correct adiabaticity parameter for a straight-line trajectory in the relativistic regime, according to Eq. (24), so the high-energy regime will also be described correctly.

B. Total cross sections

A great advantage of the straight-line trajectory approximation is that one can obtain analytic expressions for the total cross section, evaluated for all impact parameters larger that a certain minimum impact parameter b_0. Thus one obtains [2]

$$\sigma_\lambda = 4\pi\left(\frac{Z_1 e^2}{(2\lambda+1)\hbar v}\right)^2 B(E\lambda) \times \sum_\mu \frac{4\bar{G}^2_{\lambda\mu}}{(\lambda+\mu)!(\lambda-\mu)!}\left(\frac{\omega}{v}\right)^{2(\lambda-1)} g_\mu\left(\frac{\omega b_0}{\gamma v}\right), \quad (27)$$

where

$$g_\mu(\xi) = 2\pi\int_\xi^\infty \xi d\xi K^2_\mu(\xi) = \pi\xi^2\left[K_{\mu+1}(\xi)K_{\mu-1}(\xi) - K^2_\mu(\xi)\right], \quad (28)$$

according to Eq. (3.4) of Ref. [2]. For dipole and quadrupole excitations this yields

$$\sigma_{\lambda=1} = 16\pi\left(\frac{Z_1 e^2}{3\hbar v}\right)^2 B(E1)\left[\frac{1}{\gamma^2}g_0(\xi) + g_1(\xi)\right], \quad (29)$$

$$\sigma_{\lambda=2} = \frac{4\pi}{3}\left(\frac{Z_1 e^2}{5\hbar v}\right)^2 B(E2)\left(\frac{\omega}{\gamma v}\right)^2 \times \left[3g_0(\xi) + g_1(\xi)\gamma^2(1+\gamma^{-2})^2 + g_2(\xi)\right]. \quad (30)$$

At intermediate and high energies, where one can assume that $\xi_b \ll 1$, one obtains the following simple asymptotic expression for the quadrupole excitation cross section:

$$\sigma_{\lambda=2} = \frac{1}{3}\left(\frac{4\pi Z_1 e^2}{5\hbar v b_0}\right)^2 B(E2). \quad (31)$$

This expression gives a surprisingly good estimate of the cross section at high energies and it provides a simple way of testing more elaborate numerical calculations. The expression (31) shows that the high-energy cross section is insensitive to the excitation energy. One can also conclude that relativistic effects are not dramatic for $E2$ transitions because all of the γ factors that appear in Eq. (30) disappear when one takes the limit $\xi_b \to 0$.

We shall see in the next section that the large relativistic effects, which have been pointed out in the literature, are primarily caused by plotting the cross sections as a function of the beam energy T per nucleon. The cross section (31), which is proportional to v^{-2}, will therefore be very sensitive to whether one uses nonrelativistic ($v = \sqrt{2T/m}$) or relativistic kinematics [Eq. (B1)] to determine the velocity.

For completeness it is noted that some relativistic effects do survive in the dipole cross section, Eq. (29), when one takes the limit $\xi_b \to 0$ in the dipole cross section, Eq. (29),

$$\sigma_{\lambda=1} = \left(\frac{4\pi Z_1 e^2}{3\hbar v}\right)^2 B(E1)\left[2\ln\left(\frac{1.123\gamma v}{\omega b_0}\right) - \left(\frac{v}{c}\right)^2\right]. \quad (32)$$

This expression shows the well-known logarithmic dependence on γ.

VI. APPLICATIONS

Two examples of calculated cross sections are shown in Fig. 3, namely, for the dipole excitation of ^{11}Be to the low-lying $1/2^-$ state, and the quadrupole excitation of ^{42}S to the lowest 2^+ state, respectively. The cross sections are shown as functions of the beam energy. In both cases the minimum impact parameter was set to $b_0 = 14$ fm and the target was Au. The excitation energy and multipole strength of the two transitions are given in Table I, which will be discussed below.

The upper thick dashed curves in Fig. 3 show the relativistic Coulomb excitation cross section for straight-line trajectories. The solid curves are based on Coulomb trajectories and make use of the expression, Eq. (26), for the interpolating model. The lower, thin dashed curves in Fig. 3 are the cross sections one obtains by inserting $\xi_a = \omega a/v$ into the expression, Eq. (26), for the interpolating model. This is seen to be a poor approximation. Inserting instead $\xi_a = \omega a/(\gamma v)$ (the thick solid curves) one obtains a smooth transition from the low-energy to the high-energy theory.

A. Comparison to experiments

A number of Coulomb excitation experiments have been performed at intermediate energies and some of them are quoted in Table I. Those considered here are of interest because sufficient experimental information was provided to repeat the analysis. The measured cross sections, σ_{exp}, can be compared to the straight-line trajectory approximation, σ_{Strl}, and to the cross section, σ_{Coul}, obtained from the interpolating model, Eq. (26). It is seen that the latter model performs very well in

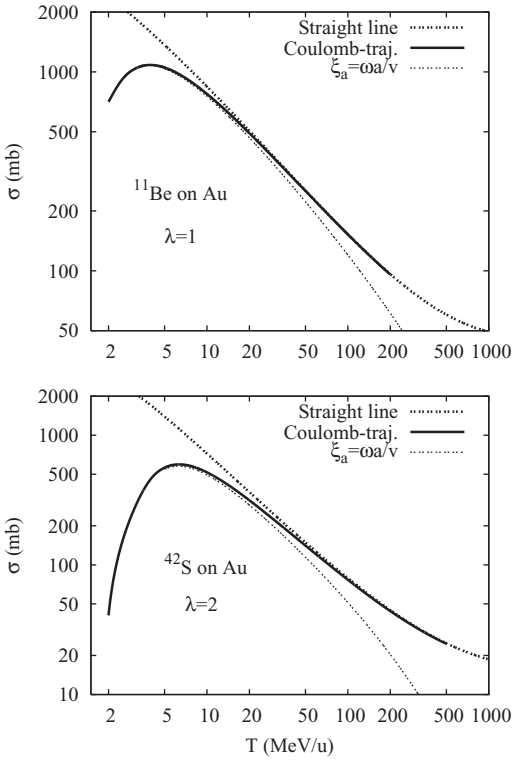

FIG. 3. Energy dependence of the relativistic cross sections for the dipole excitation of ^{11}Be and the quadrupole excitation of ^{42}S discussed in the text. The target is Au, and the minimum impact parameter was set to 14 fm in both cases. The thick dashed curves show the straight-line trajectory approximation, Eqs. (29),(30). The solid curves show the interpolating, relativistic Coulomb excitation cross section, Eq. (26). The thin dashed curves are also based on Eq. (26) but use $\xi_a = \omega a/v$ in the second argument of $K^{\rm eff}_{\lambda\mu}(b/a, \xi_a)$.

comparison to the measured cross sections. The deviations are insignificant in comparison to the experimental uncertainty.

It should be emphasized that most of the $B(E2)$ values quoted in Table I were extracted from the data using the relativistic straight-line trajectory approximation with some corrections included for the Coulomb distortion of the trajectory. The good agreement between $\sigma_{\rm Coul}$ and the measured cross sections therefore shows that the previous analyses were very reasonable. The results of the straight-line trajectory approximation, $\sigma_{\rm Strl}$, are quoted in the last column. They are typically 5 to 10% higher than the measured values.

The ratio of measured and calculated cross sections is illustrated in Fig. 4. The solid circles show the ratio $\sigma_{\rm exp}/\sigma_{\rm Coul}$ with respect to the interpolating relativistic Coulomb excitation cross section. The average ratio is about 2% less than 1. The triangles in Fig. 4 show the experimental ratio $\sigma_{\rm exp}/\sigma_{\rm Strl}$ to the relativistic straight-line trajectory calculation. Here the deviation from 1 is much larger. The deviation from the solid points reflects the significance of the Coulomb distortion of the trajectory. It amounts to about 3–9%. The largest deviations from the solid points occur in the low energy experiments, run nos. 4–8 (see Table I).

There are two examples in Table I where the $B(E2)$ values are known from other sources, namely, ^{24}Mg and ^{26}Mg.

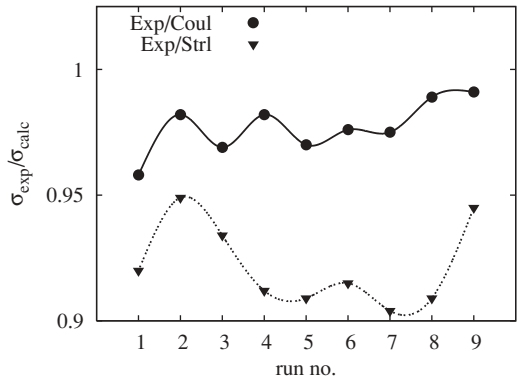

FIG. 4. Ratio of measured and calculated Coulomb excitation cross sections for the different runs shown in Table I. Shown are the results for the interpolated relativistic Coulomb excitation (solid points) and the straight-line trajectory calculations (triangles).

The calculated cross sections, $\sigma_{\rm Coul}$, are also in these cases consistent with the measured cross sections. This is very fortunate because the uncertainties are small [about 5% on the measured cross sections and 3% on the $B(E2)$ values]. These two measurements therefore provide an independent test of the interpolating model, Eq. (26).

The last example on a comparison with data is the Coulomb excitation of ^{46}Ar [13], which was measured for a range of maximum acceptance angles. The measurements are compared to two calculations in Fig. 5, namely, the straight-line and the 'interpolated' Coulomb trajectory calculation, Eq. (26). Both calculations are in good agreement with the data because the experimental uncertainties are much larger than the difference between the two calculations.

B. Comparison to other methods

The relativistic description for straight-line trajectories developed by Winther and Alder [2] was based on the Liénard-Wiechert potential. A different method was used by Aleixo and

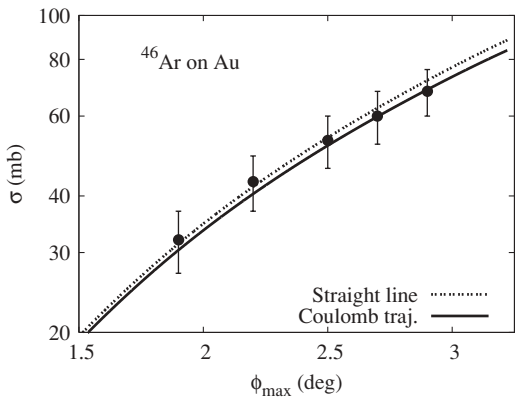

FIG. 5. Cross section for the Coulomb excitation of the 2^+ state in ^{46}Ar on a Au target at 73.2 MeV/nucleon as a function of the maximum laboratory acceptance angle $\phi_{\rm max}$. The relativistic straight-line and Coulomb trajectory calculations are compared to the data [13].

Bertulani [4] who calculated the retardation effects explicitly for Coulomb trajectories. The latter approach was used by Bertulani *et al.* [5,6] to investigate the effects of relativity and Coulomb distortions at intermediate energies in much the same way it is done here. It is therefore of interest to compare Eq. (26) to the predictions of the more elaborate theory.

An example of a comparison of calculated cross sections is shown in Fig. 6 for the Coulomb excitation of ^{46}Ar to the 2^+ on a Pb target. The input is the same as used in producing table 2 of Ref. [6], and it was assumed [15] that the distance of closest approach for a Coulomb trajectory, $r_0(b) = a + \sqrt{a^2 + b^2}$ according to Eqs. (10) and (11), has the minimum value $r_{\min} = R_1 + R_2 = 1.2(A_1^{1/3} + A_2^{1/3})$. The solid line is the cross section obtained from the interpolating model, Eq. (26). The upper dashed curve is the result for straight line trajectories with minimum impact parameter $b_{\min} = \sqrt{r_{\min}(r_{\min} - 2a)}$. The lower dashed curve is the nonrelativistic cross section for Coulomb trajectories. It is seen that the solid curve interpolates smoothly between the nonrelativistic Coulomb trajectory calculation at low energy and the relativistic straight-line trajectory calculation at high energy.

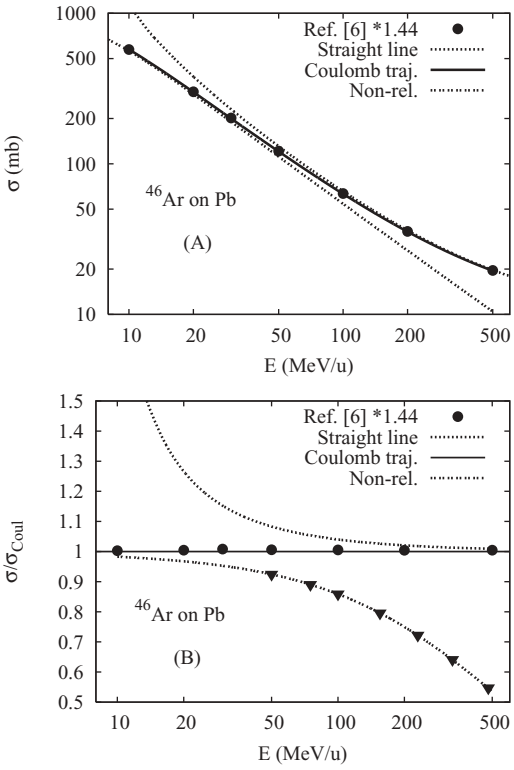

FIG. 6. (A): cross sections for the 2^+ excitation of ^{46}Ar on a Pb target. The minimum distance of closest approach was set to 11.41 fm. The relativistic straight-line (upper dashed curve) and Coulomb trajectory calculations (solid curve) are compared to the nonrelativistic Coulomb trajectory calculation (lower dashed curve), and to the results of Ref. [6] (solid points) which have been multiplied by 1.44. (B): ratios of the cross sections in (A) to the relativistic Coulomb trajectory calculation. The triangles show the estimate, Eq. (33).

The solid points in Fig. 6(a) are based on the cross sections published in table 2 of Ref. [6]. They have here been multiplied by the factor 1.44 because a factor of e^2 was unfortunately omitted [15] in the calculations of Ref. [6]. The results are presented in Fig. 6(b) in terms of the ratio to the interpolating relativistic Coulomb trajectory calculation, Eq. (26). The average value of the solid points is close to one (actually 1.005 $\pm$ 0.002, to be precise) which shows that the two theories are in excellent agreement. This may not be so surprising because both theories approach the relativistic straight-line trajectory approximation at high energy and the nonrelativistic Coulomb trajectory calculation at low energy.

The lower dashed curve in Fig. 6(b) shows that relativistic effects are enormous at 500 MeV/nucleon. It is interesting that the large relativistic effects have a very simple explanation. Thus, according to the asymptotic expression, Eq. (31), the quadrupole excitation cross section is proportional to v^{-2} at high energies. In the nonrelativistic calculation this implies $\sigma_2^{\rm NR} \propto m/(2T)$. In the relativistic calculation one obtains instead $\sigma_2^{\rm rel} \propto (m+T)^2/[T(2m+T)]$, according to Eq. (B1) of Appendix B. The ratio of the two cross sections is therefore

$$\frac{\sigma_2^{\rm NR}}{\sigma_2^{\rm rel}} \approx \frac{m(2m+T)}{2(m+T)^2}. \tag{33}$$

(There is also a difference in the minimum impact parameter in the relativistic and nonrelativistic calculations but the effect is small.) The expression (33) is illustrated in Fig. 6(b) by the triangles which explain quite accurately the behavior of the nonrelativistic calculation at high energy.

C. Significance of relativistic effects

Another way to illustrate the effects of relativity is to recalculate the cross sections shown in Fig. 3 assuming that $\gamma = 1$ everywhere in the underlying equations, Eqs. (24)–(26). The velocity v, which appears explicitly in these equations, will be determined from the relativistic expression, Eq. (B1), in order to avoid the trivial relativistic effect described by Eq. (33). The results of such calculations show that the cross sections for the excitation of the 2^+ state in ^{42}S, which were shown in Fig. 3, change by less than 0.5%, both for the straight-line trajectory calculation (24) and also for the interpolated Coulomb trajectory model, Eq. (26).

Similar calculations performed for the dipole excitation of ^{11}Be (which were shown in Fig. 3) change the cross section by less than 1% at energies below 200 MeV/nucleon. The change is about 10% at 1 GeV/nucleon but that is not so surprising because the asymptotic dipole cross section, Eq. (32), does contain a γ factor, whereas the asymptotic quadrupole cross section, Eq. (31), does not.

It is concluded that the relativistic effects in the Coulomb excitation of nuclei are large at intermediate and high energies but most of the effect is trivial and can easily be avoided by using the correct relativistic expression to determine the velocity from the beam energy. In the analysis of measurements it is also important to use relativistic kinematics when converting scattering angles into impact parameters.

The nontrivial relativistic effects on the Coulomb quadrupole excitation, on the other hand, are surprisingly small.

D. Significance of Coulomb distortion

Let us finally take a look at how the straight-line trajectory approximation can be corrected for Coulomb distortions. Two examples are shown in Fig. 7, namely, the Coulomb excitation to the 2^+ state of ^{16}N with excitation energy $E_x = 0.12\,\text{MeV}(A)$, and also to the 2^+ state of ^{54}Ni with excitation energy $E_x = 1.4\,\text{MeV}(B)$. The $B(E2)$ values were taken from table 2 of Ref. [6]. The results are shown in terms of the ratio to the interpolating, relativistic Coulomb excitation cross section, Eq. (26). The calculations were again performed with the minimum distance of closest approach $r_{\min} = 1.2(A_1^{1/3} + A_2^{1/3})$.

The comparison with Ref. [6] is illustrated in Fig. 7 by the solid points. The cross sections from table 2 of Ref. [6] were again multiplied with the factor 1.44. It is seen that the solid points are very close to 1 for the excitation of ^{54}Ni. There are some discrepancies for ^{16}N, where the average ratio is 1.028 ± 0.012. It is therefore concluded that the two theories of relativistic Coulomb excitation agree within a few percent.

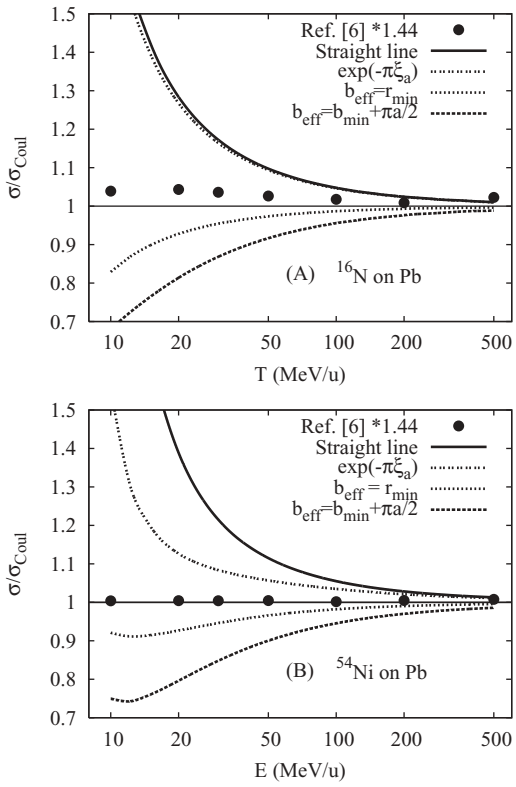

FIG. 7. Ratios of different cross sections to the relativistic Coulomb trajectory calculation. Results are shown for the excitation of the 2^+ state in ^{16}N and ^{54}Ni, respectively, on a Pb target. The thick solid curves are the ratios for the straight line trajectory approximation. The dashed curves show various ways of correcting the straight-line approximation, such as multiplying with the factor $\exp(-\pi\xi_a)$, or using the effective minimum impact parameters discussed in the text. The solid points are the ratios for the cross sections given in table 2 of Ref. [6] multiplied by 1.44.

The thick solid curves in Fig. 7 show the ratio for the relativistic straight-line trajectory approximation, and the dashed curves show the results of various ways to correct this approximation for Coulomb distortions. The top dashed curves show the straight-line approximation multiplied by the factor $\exp(-\pi\xi_a)$. This factor has a large effect for the heavier nucleus ^{54}Ni with the relatively large excitation energy but it has essentially no effect for the lighter nucleus ^{16}N with the small excitation energy.

The lowest dashed curves in Fig. 7 show the straight-line trajectory result one obtains by replacing the minimum impact parameter $b_{\min}$ by the effective value $b_{\text{eff}} = b_{\min} + \pi a/2$. This approximation was justified in Ref. [2] for large impact parameters, where the excitation probability falls off exponentially as $\exp(-2\omega b/(\gamma v))$. Thus by multiplying the excitation probability for a straight line trajectory, P_{Strl}, with the factor $\exp(-\pi\xi_a)$ one obtains approximately

$$P_{\text{Strl}} \exp(-\pi\xi_a) \propto \exp\left(-\frac{2\omega b}{\gamma v}\right) \exp\left(-\pi\frac{\omega a}{\gamma v}\right) = \exp\left[-\frac{2\omega}{\gamma v}\left(b + \frac{\pi a}{2}\right)\right].$$

This argument does not always apply to the Coulomb excitation of low-lying states at intermediate energies because the minimum impact parameter is usually much smaller than the adiabatic distance $\gamma v/\omega$. Using the effective minimum impact parameter has a very large effect on the calculated cross section. It produces a ratio in Fig. 7 that is almost as far below 1 as the ratio for the pure straight line trajectory calculation is above 1. The approximation is therefore not very useful for quadrupole excitations. It works apparently better for dipole excitations, as discussed in connection with Figs. 2 and 3, but that will not be discussed here.

The second lowest curves in Figs. 7(a) and 7(b) are the results one obtains by choosing the effective minimum impact parameter, $b_{\text{eff}} = r_{\min}$, which is the minimum distance of closest approach that is used in the relativistic Coulomb trajectory calculation. This approximation was recommended by Goldberg [16], and it is evidently the best choice out of the four examples of approximations shown in Fig. 7.

In the analysis of an actual experiment the cross section ratio discussed above would usually be closer to one because one would always choose a small acceptance angle (i.e., a large minimum impact parameter) in order to avoid the influence of nuclear and higher-order processes.

VII. CONCLUSIONS

A model has been devised for including relativistic effects in calculations of the Coulomb excitation cross section at intermediate energies. The model interpolates smoothly between the theory of nonrelativistic Coulomb excitation at low energy and the relativistic, straight-line trajectory approximation high energy. The results that were obtained with this model compare very well with the calculations performed by Bertulani *et al.*,

who included the relativistic retardation effects explicitly for Coulomb trajectories.

It was demonstrated that the large relativistic effects, which have been pointed out in the literature, are mainly caused by comparing calculations that are based on a relativistic and a nonrelativistic velocity, respectively. The nontrivial relativistic effects, which are beyond the simple relativistic kinematics of two-body scattering, are surprisingly small for quadrupole excitations.

The Coulomb distortion, which is responsible for the deviation between the straight line trajectory approximation and calculations that are based on a Coulomb trajectory, can also have a very large effect. However, the effects of the Coulomb distortion are usually suppressed by the experimental conditions and simple corrections can be made to improve the accuracy of the straight line trajectory approximation.

The proposed interpolating model reproduces fairly well the analyses that have been performed previously, primarily of quadrupole excitation experiments, at beam energies in the range of 30 to 70 MeV/nucleon. The average deviation is only a few percent. The model also reproduces the measured cross sections in the few cases where the quadrupole excitation strength is known accurately from other sources.

The good agreement with the previous analyses is partly due to the experimental conditions, which suppress the effects of the Coulomb distortion, and partly to the fact that some corrections for the distortion were made in the analyses. However, if high precision Coulomb excitation experiments were pursued, it would be necessary to treat the Coulomb distortion more accurately in the analysis. It is believed that the interpolating Coulomb excitation model proposed here would provide a sufficiently accurate description.

ACKNOWLEDGMENTS

This work was supported by the U.S. Department of Energy, Office of Nuclear Physics, under Contract No. DE-AC02-06CH11357.

APPENDIX A: STRAIGHT-LINE TRAJECTORY

In coordinate system A, a straight line trajectory has the coordinates $x(t) = b$, where b is the (constant) impact parameter, and $y(t) = vt$. Using the dimensionless integration variable $s = vt/b$, the orbital integral, Eq. (7), is therefore

$$\begin{aligned}\tilde{S}^A_{\lambda\mu} &= d^\lambda_{\mu 0}\left(\frac{\pi}{2}\right)\frac{1}{vb^\lambda}\int_{-\infty}^{\infty} ds\, e^{i\xi_b s}\frac{(1+is)^\mu}{(1+s^2)^{(\lambda+\mu+1)/2}} \\ &= d^\lambda_{\mu 0}\left(\frac{\pi}{2}\right)\frac{1}{vb^\lambda}\left(1+\frac{d}{d\xi_b}\right)^\mu\int_{-\infty}^{\infty} ds\,\frac{\cos(\xi_b s)}{(1+s^2)^{(\lambda+\mu+1)/2}},\end{aligned} \tag{A1}$$

where $\xi_b = \omega b/v$ is the adiabaticity parameter. The tilde on $\tilde{S}^A_{\lambda\mu}$ is a reminder that we are using the straight-line approximation. An analytic expression for the integral is given in the book by Gragshteyn and Ryzhik [17], Eqs. 8.432 no. 5, and one obtains

$$\tilde{S}^A_{\lambda\mu} = d^\lambda_{\mu 0}\left(\frac{\pi}{2}\right)\frac{2}{vb^\lambda}\frac{1}{(2n-1)!!}\left(1+\frac{d}{d\xi_b}\right)^\mu \xi_b^n K_n(\xi_b), \tag{A2}$$

which is expressed in terms of modified Bessel functions of order $n = (\lambda+\mu)/2$. Here $\lambda+\mu$ is even as mentioned earlier so n is an integer. We can express the result in a form similar to Eq. (12) with

$$\tilde{I}_{\lambda,\pm\mu} = \frac{2}{(2n-1)!!}\left(\frac{a}{b}\right)^\lambda\left(1\pm\frac{d}{d\xi_b}\right)^\mu \xi_b^n K_n(\xi_b). \tag{A3}$$

To evaluate this expression one can make use of the relations: $\frac{d}{dx}(x^n K_n(x)) = -x^n K_{n-1}(x)$. For dipole and quadrupole excitations one obtains

$$\tilde{I}_{1,\pm1} = 2\xi_a[K_1(\xi_b) \mp K_0(\xi_b)], \tag{A4}$$

$$\tilde{I}_{20} = \xi_a^2[K_2(\xi_b) - K_0(\xi_b)] = 2\left(\frac{a}{b}\right)^2\xi_b K_1(\xi_b), \tag{A5}$$

$$\tilde{I}_{2\pm2} = \frac{1}{3}\xi_a^2[K_2(\xi_b) \mp 4K_1(\xi_b) + 3K_0(\xi_b)], \tag{A6}$$

where the relation $K_2(x) = K_0(x) + 2/x\,K_1(x)$ has been used in Eq. (A5).

To improve the straight-line approximation, one can multiply the results, Eqs. (A4)–(A6), by the factor $\exp(-\pi\xi_a/2)$, according to Winther and Alder [2]. In fact, the exact analytic expression, which has been obtained for a Coulomb trajectory in the case of dipole excitations, supports this suggestion; see Eq. (12) in appendix H of Ref. [1]. We will later on investigate how good this improvement and other approximations are for quadrupole excitations.

APPENDIX B: RELATIVISTIC KINEMATICS

Here we specify the expressions that are used to calculate the relativistic Coulomb scattering. Most of them are taken from Jackson's book [18]. First of all, the kinetic energy T of the projectile is commonly given in units of MeV/nucleon so the γ factor and the beam velocity v can be obtained from

$$\gamma m = m + T, \quad \beta = v/c = \frac{\sqrt{T(2m+T)}}{m+T}, \tag{B1}$$

where $m = 931.5$ MeV is the nucleon mass (using the notation $c = 1$).

The masses of projectile and target are denoted by M_1 and M_2, and the total energy in the center of mass system is [Jackson (12.31)]

$$E' = \sqrt{M_1^2 + M_2^2 + 2\gamma M_1 M_2}.$$

where γM_1 is the laboratory energy of the projectile. Moreover, the energy and momentum of the projectile in the center of mass system are [Jackson, Eqs. (12.31–34)]

$$E'_1 = \frac{M_1^2 + E_1 M_2}{E'} = \frac{M_1(M_1+\gamma M_2)}{E'},$$

$$p'_1 = \frac{M_2}{E'}p = \frac{M_1 M_2}{E'}\gamma v,$$

where $p = \gamma M_1 v$ is the momentum of the projectile in the laboratory frame. Note that the nonrelativistic reduced mass $M_1 M_2/(M_1 + M_2)$ has been replaced in the last expression by the relativistic reduced mass,

$$M_0 = \frac{M_1 M_2}{E'} = \frac{M_1 M_2}{\sqrt{M_1^2 + M_2^2 + 2\gamma M_1 M_2}}. \tag{B2}$$

Rutherford's scattering formula in the center-of-mass system is derived from the transverse momentum transfer in elastic Coulomb scattering, estimated in the straight line approximation by

$$\Delta p_\perp = p_1' \sin(\theta) = \frac{2 Z_1 Z_2 e^2}{v b}.$$

This is a reasonable approximation in high-energy forward-angle scattering but to match the nonrelativistic expression, $\tan(\theta/2) = a/b$, one should consider the Coulomb distortion of the trajectory. This would give a factor of $\cos^2(\theta/2)$ on the right-hand side, so we obtain

$$\tan(\theta/2) = \frac{Z_1 Z_2 e^2}{p_1' v b} = \frac{Z_1 Z_2 e^2}{\gamma M_0 v^2 b}.$$

Thus we recover the usual scattering formula, $\tan(\theta/2) = a/b$, but the definition of a, Eq. (4), must be replaced by

$$a = \frac{Z_1 Z_2 e^2}{\gamma M_0 \beta^2}. \tag{B3}$$

There are two corrections compared to Eq. (4). One is the factor $1/\gamma$, which is commonly considered. The other is the relativistic reduced mass M_0, which is often replaced by the nonrelativistic value.

The scattering angle in the laboratory frame is determined by [see Jackson (12.50)]

$$\tan(\phi) = \frac{\sin(\theta)}{\gamma_{\text{c.m.}}(\cos(\theta) + \alpha)}, \tag{B4}$$

where $\gamma_{\text{c.m.}} = (\gamma M_1 + M_2)/E'$ [Jackson (12.35)], and

$$\alpha = \frac{M_1}{M_2} \frac{M_1 + \gamma M_2}{\gamma M_1 + M_2}, \tag{B5}$$

according to Jackson (12.54) for elastic scattering. It is seen that the transformation from the c.m. to the laboratory system reduces to the usual nonrelativistic expression for $\gamma \to 1$.

[1] K. Alder and A. Winther, *Electromagnetic Excitation* (North-Holland, New York, 1975).
[2] A. Winther and K. Alder, Nucl. Phys. **A319**, 518 (1979).
[3] T. Glasmacher, Annu. Rev. Nucl. Part. Sci. **48**, 1 (1998).
[4] A. N. F. Aleixo and C. A. Bertulani, Nucl. Phys. **A505**, 448 (1989).
[5] C. A. Bertulani, A. E. Stuchbery, T. J. Mertzimekis, and A. D. Davies, Phys. Rev. C **68**, 044609 (2003).
[6] C. A. Bertulani, G. Cardella, M. D. Napoli, G. Raciti, and E. Rapisarda, Phys. Lett. **B650**, 233 (2007).
[7] H. Scheit, A. Gade, Th. Glasmacher, and T. Motobayashi, Phys. Lett. **B659**, 515 (2007).
[8] K. Alder, A. Bohr, T. Huus, B. Mottelson, and A. Winther, Rev. Mod. Phys. **28**, 432 (1956).
[9] P. D. Cottle *et al.*, Phys. Rev. C **64**, 057304 (2001).
[10] Evaluated Nuclear Structure Data Files (ENSDF), National Nuclear Data Center, Brookhaven National Laboratory, http://www.nndc.bnl.gov/
[11] J. A. Church *et al.*, Phys. Rev. C **72**, 054320 (2005).
[12] H. Scheit *et al.*, Phys. Rev. Lett. **77**, 3967 (1996).
[13] A. Gade *et al.*, Phys. Rev. C **68**, 014302 (2003).
[14] M. Fauerbach *et al.*, Phys. Rev. C **56**, R1 (1997).
[15] C. A. Bertulani (private communications).
[16] A. Goldberg, Nucl. Phys. **A240**, 636 (1984).
[17] I. S. Gradshteyn and I. M. Ryzhik, *Table of Integrals, Series and Products* (Academic Press, New York, 1965).
[18] J. D. Jackson, *Classical Electrodynamics* (Wiley, New York, 1967).